

# An approach for failure analysis of composite bridge deck systems with openings

Lei Zhao<sup>†</sup>

*Department of Civil and Environmental Engineering, University of Central Florida,  
Orlando, FL 32816-2450, USA*

Vistasp M. Karbhari<sup>‡</sup>

*Department of Structural Engineering, University of California San Diego, MC-0085,  
La Jolla, CA 92093-0085, USA*

*(Received August 31, 2004, Accepted March 2, 2005)*

**Abstract.** Design details pertaining to the connection between some recently developed fiber reinforced polymer (FRP) composite deck systems and the supporting girders require openings through cells of the deck. This significantly changes the stress distribution in these components. As a result, the conventional assumptions that deck designs are controlled by their stiffness, and not strength, needs a closer examination. This paper proposes an analytical method to investigate the stress states and failure mechanisms using a type of “global-local” modeling perspective, incorporating classical lamination theory and first ply failure criterion with use of appropriate stress concentration factors around the cutouts. The use of a “smeared-stress” approach is presented as a potential means of simplifying certain FRP specific complexities, while still enabling prediction of overall failure.

**Key words:** decks; finite element analysis; cutout; stress concentration; first-ply failure.

---

## 1. Introduction

Fiber reinforced polymer (FRP) composite bridge decks show significant potential for use as both replacement decks on existing girders and as part of new structural systems due to their lightweight, tailorable properties and potential long-term durability. Beginning with the Ginzi bridge in Bulgaria built in 1981 and the Miyun bridge in China in 1982, a variety of deck concepts have been developed ranging from the use of honeycomb sandwich panels (Walker 1998, Stone *et al.* 2001) and truss type panels (Karbhari *et al.* 1997) to the use of cellular type modular sections (Karbhari *et al.* 1997, Head 1998, Lopez-Anido *et al.* 1998). Summaries of applications (Bakis *et al.* 2002, Holloway and Head 2001, Loud and Kliger 2001) and analytical developments (Zureick *et al.* 1985) have been reported earlier and hence will not be repeated herein. To date designs have necessarily been controlled by the deflection limit state rather than the strength limit state (Henry 1985, Plecnik

---

<sup>†</sup> Assistant Professor, Corresponding author, E-mail: leizhao@mail.ucf.edu

<sup>‡</sup> Professor

and Azar 1991, Karbhari and Seible 2000) resulting in significant strength over-capacity. Based on a series of static and fatigue tests conducted on deck panels fabricated from pultruded FRP components Temeles (2001) concluded that the maximum strain level was less than 15% of the ultimate tensile strain in the weaker direction and that the systems had safety factors in excess of 8 with respect to legal truck loads.

Notwithstanding the fact that current FRP deck systems are stiffness controlled there is a need for factors of safety both to address long-term environmental durability and aspects associated with damage tolerance. Although there is currently a lack of substantiated data pertaining to deck system durability, existing standards such as BS 4994 (1987) or even ASME RTP-1 (1998), which prescribe large factors of safety (6-12), could be used to provide conservative designs. The use of approaches such as suggested in the aforementioned specifications provide substantially increased thicknesses leading to both very low stress levels and even sacrificial material which if deteriorated through long-term environmental exposure would have no discernable effect on the response at the materials and structural levels. However, aspects such as holes and attachments for connecting these decks to the supporting girders have not been adequately addressed, especially as related to the effect of stress concentrations around these local areas which could effectively nullify the apparent large over-strength of the system as a whole. This paper investigates the effect of one class of connections on stress states and failure mechanisms.

The example considered relates to the attachment of cellular pultruded deck panels to concrete filled carbon/epoxy girders through encapsulation of dowels, the ends of which are confined in the girders, in cutouts in the deck providing a positive connection between the components. The proposed method of analysis uses a global-local approach. At the local level, stiffness properties, which are later used as inputs to the global model, are established using classical lamination theory (CLT) considering the exact lay-up used in the deck with strength being determined based on sequential use of the first-ply failure theory incorporating stress concentration factors around holes. At the global level a 3-D finite element analysis model is used to assess deformation response and stress distribution, which is then used in a local model to predict locations of high stress and modes of failure. The proposed methodology provides ease of use for conventional bridge designers while enabling the incorporation of aspects specific to FRP composites such as interlaminar stresses (which cause delaminations) and stress concentrations around cutouts.

## 2. Test system and experimental results

The bridge system considered in this investigation was developed for implementation on the Kings Stormwater Channel Bridge (Seible *et al.* 1999), a 20.1 m two span beam and slab bridge with a multi-column intermediate pier (Fig. 1). The superstructure consists of concrete-filled circular carbon/epoxy filament wound shells, connected to a modular E-glass/polyester-vinylester pultruded core deck system. The carbon/epoxy shells, of 0.342 m inside diameter with 10 mm wall thickness, serve the dual functions of reinforcement and stay-in place formwork for concrete. The concrete provides anchorage to the steel dowels that are used for deck-to-girder connections and also stabilizes the shell wall against local buckling, thereby enabling the use of thin wall thicknesses (Seible *et al.* 1999, Karbhari *et al.* 2000). The deck is assembled of pultruded cores that are bonded together (Fig. 2) and stiffened with additional face-sheets. The direction of the pultruded core elements, representing the principal direction of the deck, is perpendicular to that of the girders.

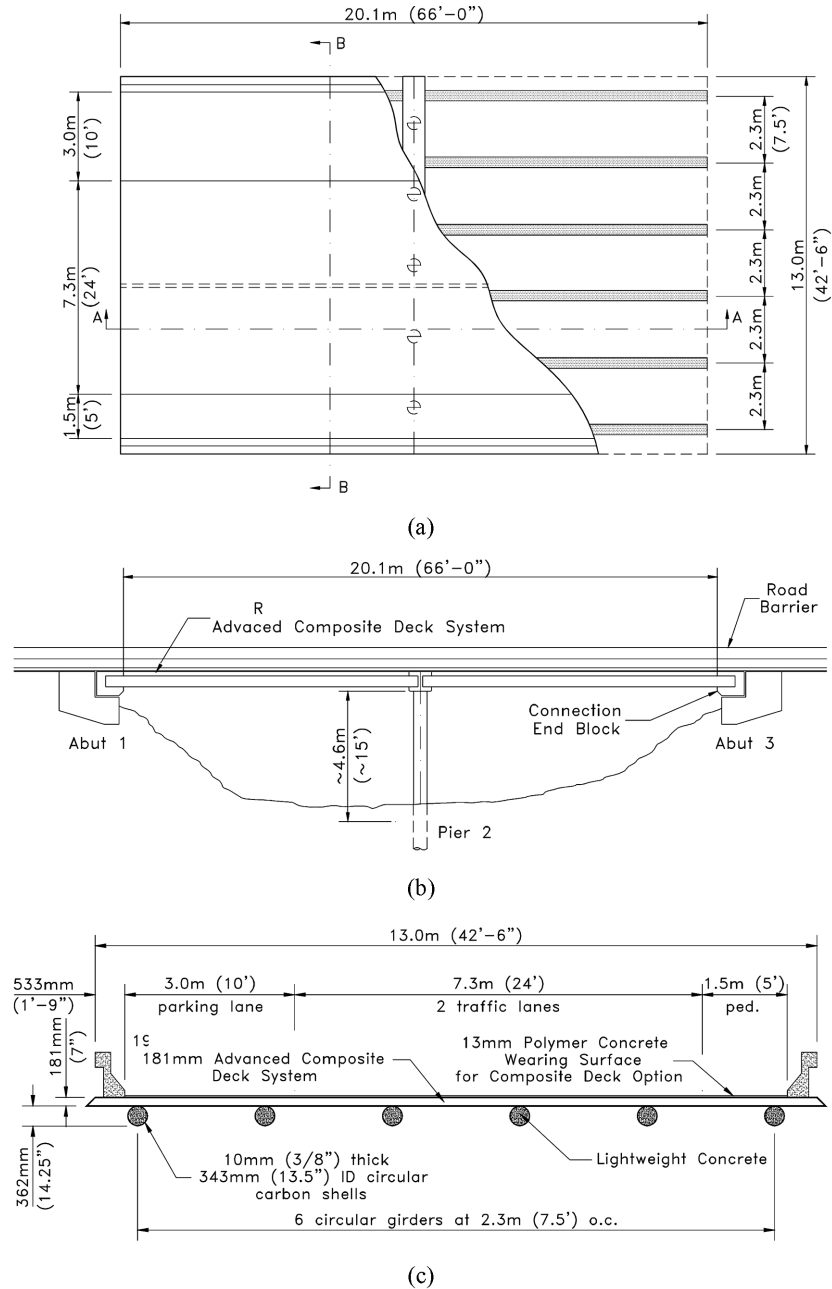
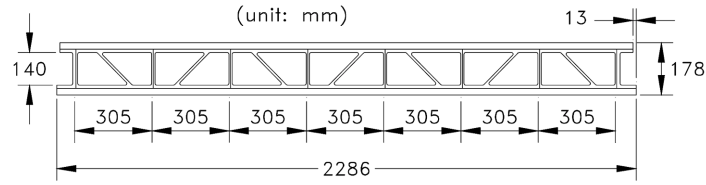


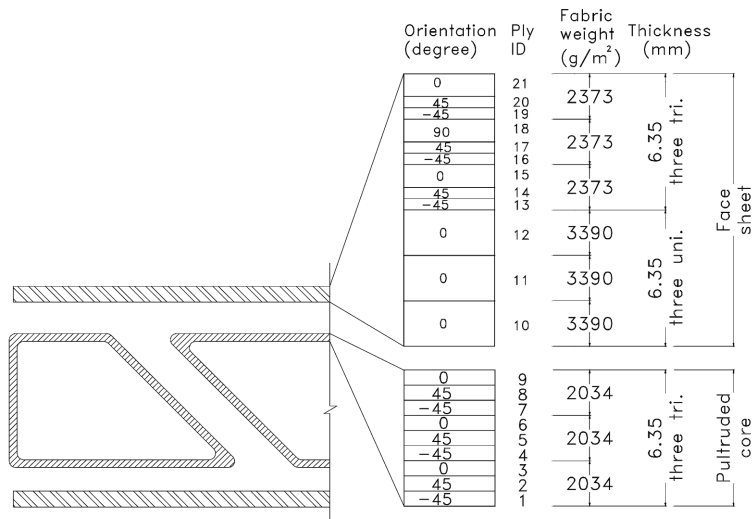
Fig. 1 Geometry of the Kings Stormwater Channel Bridge (a) Plan view, (b) Longitudinal section (Section A-A in Fig. 1a), (c) Cross section (Section B-B in Fig. 1a)

Details related to experimental structural characterization of the components and the system is reported by Karbhari *et al.* (2000) and hence are not repeated herein.

The deck-to-girder connection is critical to the successful implementation and long-term durability of the bridge system. In the present case a connection is achieved with U-shaped mild steel dowel



Cross-Sectional View of Pultruded Profiles With Face-Sheets



Exploded View Showing Different Elements (Gaps are for purposes of illustration only. Actual components are adhesively bonded)

Fig. 2 Schematic of deck system showing components and fabric lay-up

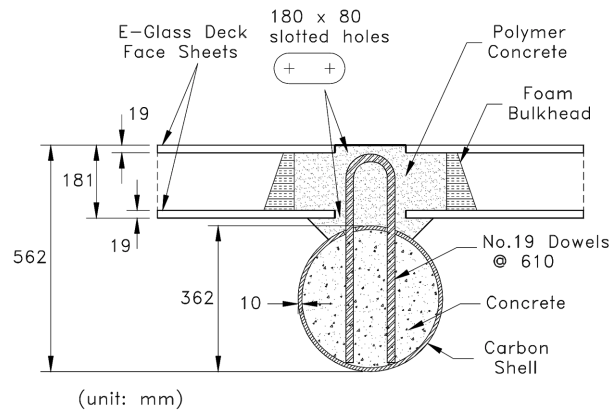


Fig. 3 Schematic of girder-deck connection detail

bars embedded in the confined concrete core of the girders and anchored into locally grouted cells of the cellular deck panels (Fig. 3). A 45° saddle formed of polymer concrete simultaneous with the filling of the local deck cells links the curved surface of the girder to the flat deck soffit. The

selection of the connection detail was made after substantial analytical and experimental investigation (Zhao 1999).

It is noted that although this form of connection provides a strong joint between the superstructure components, it also incorporates the use of cut-outs in the components, which can be sources of edge-induced layer separations (delaminations) and stress-concentrations which, due to the layered structure of the fiber reinforcement and its intrinsic anisotropy, can be significantly different from the conventionally used factor of 3 in metals. As shown in Fig. 3 the design of the girder-to-deck connection incorporates cutouts in both the deck and the girders. In the decks the cutouts are of size 180 mm × 80 mm, with semi-circular ends in the longer direction, in the top and bottom flanges. The long-direction is aligned with the direction of the pultruded core. The holes in the bottom flange enable the dowels, which are grouted into the carbon/epoxy girders, to be inserted into the deck, whereas the cutouts in the top flange allow the polymer concrete to be poured into the cell to form the shear connection. Being along the compression flange in bending these cutouts could significantly affect the local stress state. These cutouts also allow for the installation of bulkheads to localize the areas to be filled with polymer concrete, thereby enabling most of the deck core to remain hollow. In the carbon/epoxy girders the cutouts are a pair of circular holes 40 mm in diameter along the top surface. These enable placement of the U-shaped dowels into the girder prior to filling it with concrete. Due to the close proximity of these holes to the neutral axis of the superstructure system in bending the stress condition around the holes is minimal and does not govern failure.

### **3. Analytical model development**

In order to enable use of a finite element analysis procedure for the prediction of both global superstructure response, as needed by bridge designers, and local response around stress concentrations, as needed at the FRP composites level, a global-local approach was used. The analytical formulation used herein assumes that:

- In-plane properties of the FRP composite dominate the behavior of the laminates in the flanges and webs of the deck;
- Interlaminar shear failure modes between layers of fabric in the pultruded profiles can be neglected. Detailed investigations showed that the maximum interlaminar shear stress was of the order of 1.4 MPa whereas the resin itself has a shear strength of 90 MPa (Zhao 1999);
- Flange and web regions between nodes (flange-to-web joints) behave as orthotropic plates and their elastic properties can be estimated using Classical Lamination Theory (CLT). Since the layup in pultruded profiles considered in such structures consists of layers of fabric, rather than just a set of unidirectional rovings, the structure is essentially a layered (or laminated) composite and hence can be appropriately modeled using classical lamination theory (CLT). It is noted that micrographs of sections show clear distinction between layers without extensive crushing and inter-penetration of roving between adjacent layers, thereby maintaining the layered structure required for use of CLT. It is further noted that the fabrics used in the pultruded profiles in the current investigation were non-woven architectures, essentially ensuring that fibers themselves were not crimped;
- Application of the maximum stress criterion in a first-ply-failure setup is sufficient to capture global failure;

- Failure can be caused by one of five stress conditions, i.e., in-plane tension and compression in the two primary directions and in-plane shear;
- Buckling stress far exceed the strength of the laminates in the configuration studied and hence this mode of failure can be neglected. This mode was extensively investigated in Zhao (1999); and
- Thermal stresses developed as a result of process cool-down can be neglected for the purposes of the present analysis.

The method of overall analysis is summarized in four steps as listed below:

1. CLT is used to estimate the elastic properties, ( $E_1$ ,  $E_2$ ,  $G_{12}$ ,  $\nu_{12}$ , etc.) of the flange and web sections. “Smear strengths” of the laminates under various loading conditions are derived using the first ply failure criterion;
2. Factors representing the stress concentration factors around each cut-out are estimated separately and incorporated into the smeared strength obtained in Step (1), and a “reduced smeared strength” is obtained for each structural element;
3. A 3-dimensional finite element model is constructed to estimate the system behavior and stress demands. The flanges and webs of the deck are treated as orthotropic plates with properties as determined in Step (1). Shell elements are used for the deck panels, and beam elements are used for the girders. The results of the analysis are used to identify the locations of potential failure and to estimate stress demands in the orthotropic composite components on the deck system;
4. The stress demands are then compared with the reduced smeared strength obtained in Step (2). The load capacity of the system corresponding to the first ply failure level of the laminate is determined and used to estimate the stress level that matches the “reduced smeared strength” of the appropriate laminate.

The objective of this procedure is to provide civil engineers and bridge designers, who may have limited knowledge of the intricacies of FRP materials, a simplified methodology of analyzing a structure without significantly changing present FEA procedures for superstructure.

### 3.1 Determination of elastic properties of representative orthotropic plates

Fig. 2 provides both an overall cross-section of the pultruded profiles with face sheets and an exploded view of a representative cross-section enabling identification of the fabric layers constituting the assembly. As depicted in Fig. 2 the deck can be considered to consist of flange and web regions. Each flange region consists of the top (or bottom) of the pultruded core, and a face sheet section, whereas each web consists of two identical core faces placed back to back. It is noted that the pultruded core is formed of three layers of a stitched non woven tri-axial fabric consisting of 33% fibers in the  $0^\circ$  direction and 67% of the fibers in the  $\pm 45^\circ$  orientation, with each layer of nonwoven fabric of  $0/\pm 45$  architecture having a basis weight of  $2034 \text{ g/m}^2$ . The face sheets consist of three inner layers of unidirectional fabric, each of aerial weight  $3390 \text{ g/m}^2$  and 3 layers of triaxial fabric ( $0/\pm 45$  architecture) of weight of  $2373 \text{ g/m}^2$  each with 50% of the fibers oriented at  $0^\circ$  and 50% at  $\pm 45^\circ$ .

Classical Lamination Theory is used to calculate the elastic properties  $E_1$ ,  $E_2$ ,  $G_{12}$ , and  $\nu_{12}$  of representative orthotropic plates, for the web and flange, respectively. The properties of the constituent materials were obtained from the data bank of the composite analysis software

Table 1(a) Ply properties of various fabrics used in the deck panel

Fabric type	Weight g/m <sup>2</sup>	Ply ID	$V_f$	$E_1$ GPa	$E_2$ GPa	$G_{12}$ GPa	$\nu_{12}$
Triaxial	2373	13-21	0.449	34.41	9.53	2.84	0.30
Uni-	3390	10-12	0.641	47.64	14.51	4.59	0.26
Triaxial	2034	1-9	0.384	29.95	8.41	2.46	0.31

Table 1(b) Orthotropic properties of laminates (Determined Through CLT)

Properties	Flange	Web
$E_1$ (GPa)	27.5	15.6
$E_2$ (GPa)	13.5	9.7
$G_{12}$ (GPa)	2.3	6.5
$\nu_{12}$	0.39	0.56

Composite Pro version 2.1: (1) E-glass has a Young's modulus of 72.4 GPa, a tensile strength of 1.86 GPa, a compressive strength of 1.10 GPa, and a Poisson's ratio of 0.2; (2) polyester resin has a Young's modulus of 3.38 GPa, a shear modulus of 1.17 GPa, a tensile strength of 75.8 MPa, a compressive strength of 372 MPa, and a Poisson's ratio of 0.38. The ply properties are obtained using the well known formulae prescribed by Hahn (Vinson and Sierakowski 2002). It is assumed that the thickness of each ply (unidirectional fiber lamina) in a layer of non-woven fabric (combinations of plies with different orientations stitched together) is proportional to the weight percentage of fibers in that layer and all plies have the same fiber volume fraction. For example, if the lay-up of a layer of fabric can be defined as  $[0^\circ (50\%)/\pm 45^\circ (50\%)]$ , the layer can be divided into three unidirectional plies oriented at  $0^\circ$ ,  $+45^\circ$ , and  $-45^\circ$ . The thickness of the  $0^\circ$  ply is 50% of the total thickness of the layer,  $t$ , whereas those of the  $+45^\circ$  and  $-45^\circ$  plies each are 25% of the total thickness. Fiber volume fraction,  $V_f$ , in each layer of fabric is determined as  $[0.001 W/(t \cdot \gamma)]$  where  $W$  is the aerial weight of the fabric in g/m<sup>2</sup>,  $t$ , is the layer thickness in mm and  $\gamma$  is the specific gravity of the fiber. For example, the "70 oz triaxial" fabric used as the top layer in the deck panel has a fiber areal weight  $W = 2373$  g/m<sup>2</sup> and a thickness of 2.12 mm. Therefore, the volume fraction of that portion of the composite can be determined as  $0.001 \times 2373/(2.12 \times 2.5) = 0.45$ . Fabric weight, ply IDs, and ply thickness are given in Fig. 2. The calculated ply properties and the elastic properties of the orthotropic plates representing the flange and web regions, based on properties of the fiber and resin, are listed in Tables 1(a) and 1(b), respectively. It should be noted that the "flange" region includes both the flange of the pultruded profile and the additional face sheet. The theoretically predicted values were found to be within 10% of the values determined experimentally through testing of coupons cut from individual sections of the deck (Zhao 1999). Considering the inherent scatter in the experimentally determined values and the good comparison between theoretical and experimental results, the theoretical values are used in further analyses.

### 3.2 Smear strength

In composite laminates stress levels vary from one layer to the next based on fiber orientation. Thus, although equivalent orthotropic properties can be easily computed and are useful in a global

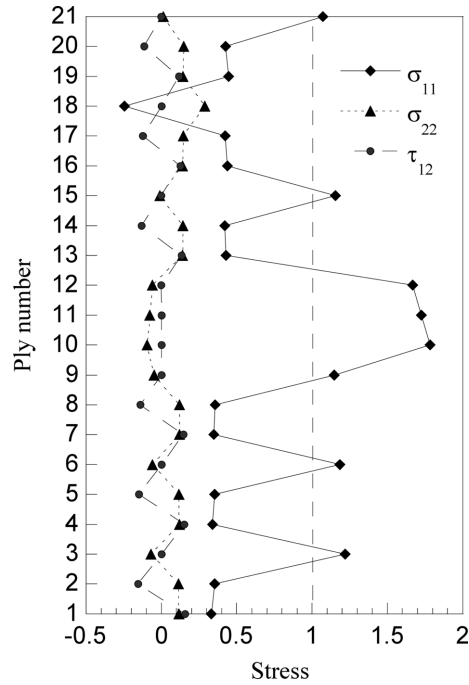


Fig. 4 Stress distribution by layer when a unit smeared stress ( $\sigma_0 = 1$ ) is applied in the  $0^\circ$ -direction in the flange section

stiffness sense, these properties can cause the designer to have a false sense of safety since through-thickness variations of in-plane stresses are neglected. Assuming the application of a unit average stress in the  $0^\circ$  direction of the flange principal in-plane stresses in each ply can be determined as shown in Fig. 4. It can be seen that the local stresses in the  $0^\circ$  plies in the fiber direction,  $\sigma_{11}$ , are magnified above the input level whereas those in the “off-axis” oriented layers are lower. For convenience of use in bridge design and analysis a parameter termed the “smeared stress” of a laminate is defined in this study as the average stress in a laminate weighted by the ply thickness ( $\sigma_{\text{smeared}} = \sum \sigma_i t_i / t$ , where  $\sigma_i$  and  $t_i$  are the stress and thickness associated with the  $i$ th ply, respectively, whereas  $t$  is the total thickness). In similar vein the “smeared strength”,  $\sigma_s$ , is defined as the average stress level associated with occurrence of first ply failure. Using the maximum stress criterion, for simplicity, the magnitude of stresses associated with first ply failure of the flange laminate under the five loading conditions can be determined as shown in Fig. 5 such that:

- A smeared tensile stress,  $\sigma_s$ , of 208 MPa in the  $0^\circ$ -direction causes matrix tension failure in Ply 18;
- A smeared tensile stress,  $\sigma_s$ , of 56.5 MPa in the  $90^\circ$ -direction causes matrix tension failure in Ply 10;
- A smeared compressive stress,  $\sigma_s$ , of 348 MPa in the  $0^\circ$ -direction causes fiber compression failure in Ply 3;
- A smeared compressive stress,  $\sigma_s$ , of 235 MPa in the  $90^\circ$ -direction causes fiber compression failure in Ply 18; and
- A smeared shear stress,  $\sigma_s$ , of 97.9 MPa in the  $0^\circ$ -direction causes matrix tension failure in Ply 19.

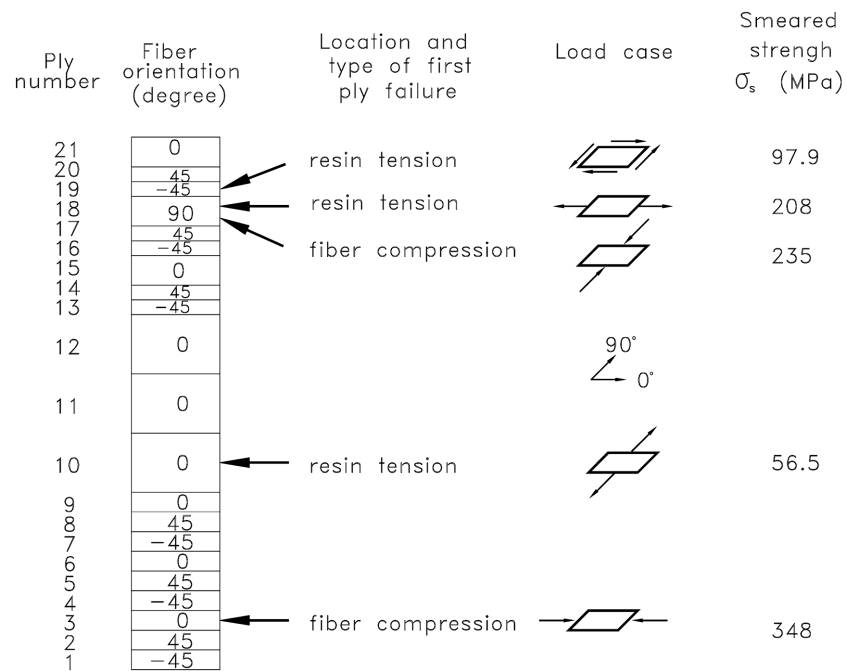


Fig. 5 Representation of in-plane stresses associated with first-ply failure modes in a representative flange laminate

### 3.3 Consideration of stress concentrations

Stress concentration factors around circular holes in orthotropic plates (with or without inclusions such as represented by the polymer concrete in-fill) are functions of the fiber orientations, and hence of the orthotropic properties of the representative laminate. Closed form solutions for those around circular and elliptical cutouts are listed in Lekhnitskii (1968) whereas those for other geometries can be easily estimated using the finite element method. The stress concentration factors for the orthotropic plates with three representative types of cutout shapes (slotted, rectangular, and circular), both with and without the appropriate inclusion materials, are summarized in Table 2. The finite element mesh of an orthotropic plate with a slotted cutout and an inclusion, which is the closest approximation of that used in the experimental investigation, is shown in Fig. 6. The unshaded area simulates the top flange of the deck panel near the cutout region, and the shaded area simulates the

Table 2 Summary of stress concentration factors (The inclusion has  $E = 25$  MPa and a Poisson's ratio of 0.2)

Cut-out geometry	Load direction			
	90°		0°	
	Without inclusion	With inclusion	Without inclusion	With inclusion
Slotted (18 × 8 cm)	3.62	1.16	2.22	1.40
Rectangular (18 × 8 cm)	3.09	1.15	2.21	1.60
Circular (8 cm diameter)	2.22	1.06	2.54	1.27

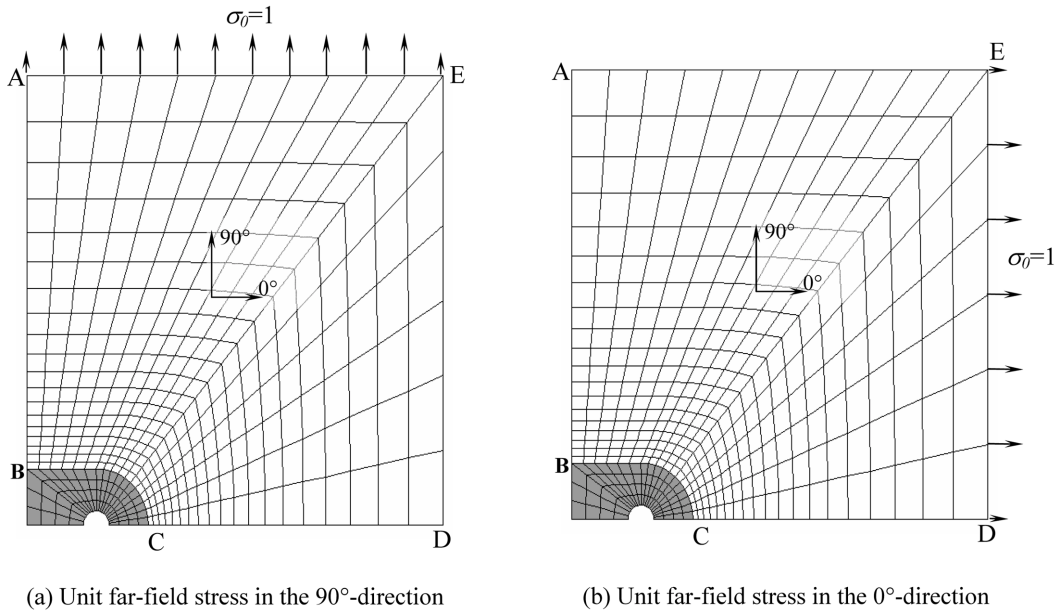


Fig. 6 FE model used to evaluate the stress concentration around a slotted cut-out

polymer concrete in-fill (with a modulus of 25 MPa and a Poisson's ratio of 0.2) used locally for the girder-to-deck connection. The 0°-direction coincides with the strong direction of the deck and the 90°-direction coincides with that of the girders of the bridge system. The stress-concentration factors in the 90°-direction can be determined by applying far-field in-plane uniform stresses to the boundary *AE* while the other boundary, *CD*, is maintained as the plane of symmetry. The stress concentration factor in the 90°-direction can be similarly obtained by applying a far-field uniform stress in the 0°-direction while maintaining the other boundary, *AB*, as the plane of symmetry. As can be seen if the addition of polymer concrete is such that it completely fills the cutout area, the stress-concentration factors are significantly reduced. However, experimental observation, both in the laboratory and field, indicates that full contact between the polymer concrete and the top flange of the deck cannot be guaranteed due to shrinkage of the polymer concrete and unevenness in the FRP laminate. Thus the positive aspects of stress alleviation through the inclusion cannot be counted on and hence for purposes of analysis the presence of the inclusion could be neglected. In the finite element model, under these circumstances, a very small Young's Modulus value, sufficient to enable computations but without causing changes in response, is assigned to the shaded area representing the inclusion. As a result, when a unit smeared stress ( $\sigma_0 = 1$ ) is applied in the 90°-direction, the maximum positive (same sign as loading stress) normal stress (magnitude 3.62) occurs at Point *C*, and the corresponding maximum negative (opposite sign to loading stress) stress (magnitude  $-1.21$ ) occurs at Point *B*. The effect of the stress concentration factor is reflected through the application of the factor to the smeared strength,  $\sigma_s$ , to provide a reduced smeared strength,  $\sigma_s'$ , as defined in Table 3. The values of the reduced smeared strength can then be used in the appropriate local regions of the structure to reflect the effects of cutouts on the local stress state.

Table 3 Summary of reduced smeared strength factors

Load case	Location	SCF <sup>1</sup>		Smeared strength <sup>2</sup> $\sigma_s$ (MPa)	Reduced smeared strength $\sigma_s'$ (MPa)	Failure mode	
		Direction				Mechanism	Direction
		0°	90°				
1	B	-1.21 <sup>3</sup>	0	207	-171	Resin tension	0°
	C	0	3.62	-235	-65	Fiber compression	90°
2	B' <sup>4</sup>	2.22	0	-348	-157	Fiber compression	0°
	C	0	-0.77 <sup>5</sup>	57	-74	Resin tension	90°

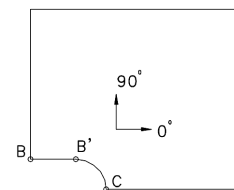
<sup>1</sup>Stress concentration factor

<sup>2</sup>(+) in tension; (-) in compression

<sup>3</sup>(-) stress concentration factor obtained by observing compressive stress in the 0° direction at location B due to a (+) unit far-field tensile stress in the 90° direction

<sup>4</sup>Location B' is at the joint of the straight and curved boundaries

<sup>5</sup>(-) stress concentration factor obtained by observing compressive stress in the 90° direction at location C due to a (+) unit far-field tensile stress in the 0° direction



### 3.4 Systems analysis

The analysis is carried out on an assemblage of the actual bridge section representing one-half of the width of the bridge and a length representing the distance between inflection points in the actual structure to provide a setup that could also be tested at full-scale. Details of experimental characterization are provided in Karbhari *et al.* (2000) and hence are not repeated herein. The assemblage consists of the deck section supported on three girders with the ends of the three girders embedded in reinforced concrete end-blocks, which are then simply supported by 6 load cells to simulate the boundary conditions. The loads are applied to the top of deck system at four locations, which are spaced at 1.8 m and 2.4 m in the *x* and *y* directions. A schematic of the test setup is shown in Fig. 7(a) and a simplified illustration of the boundary conditions at the ends of the girders is shown in Fig. 7(b). The system is pin-supported at locations A, C, and E, and roller-supported at locations B, D, and F. The “arrows” denote the fixed translational Degrees of Freedom (DOF) and the “circle-arrows” denote the fixed rotational DOF.

Vertical loads of magnitude P (at each loading point) are applied to the center of the system at four locations with spacings of 2.4 m in the longitudinal (girder) direction and 1.8 m in the transverse direction. A global finite element model is created using ABAQUS, with four-node reduced integration shell elements (ABAQUS Type: S4R5) being used for the flanges and webs of the FRP composite deck panels, and three-dimensional beam elements (ABAQUS Type: B31) being used for the concrete-filled carbon shell girders. The girder-to-deck connections are modeled with non-linear spring elements. The shear force transferred between the girders and deck is simulated by forces in the spring and slippage between the girder and deck is simulated by the deflection of the spring. Rigid links are used to maintain the relative distance between the deck and the center of the girders, and rigid beams are used to maintain displacement compatibility between the nodes of the beam elements and the spring elements. A rigid beam element constrains the three rotational degrees of freedom (DOF) of the two nodes it connects, while maintaining compatibility of the

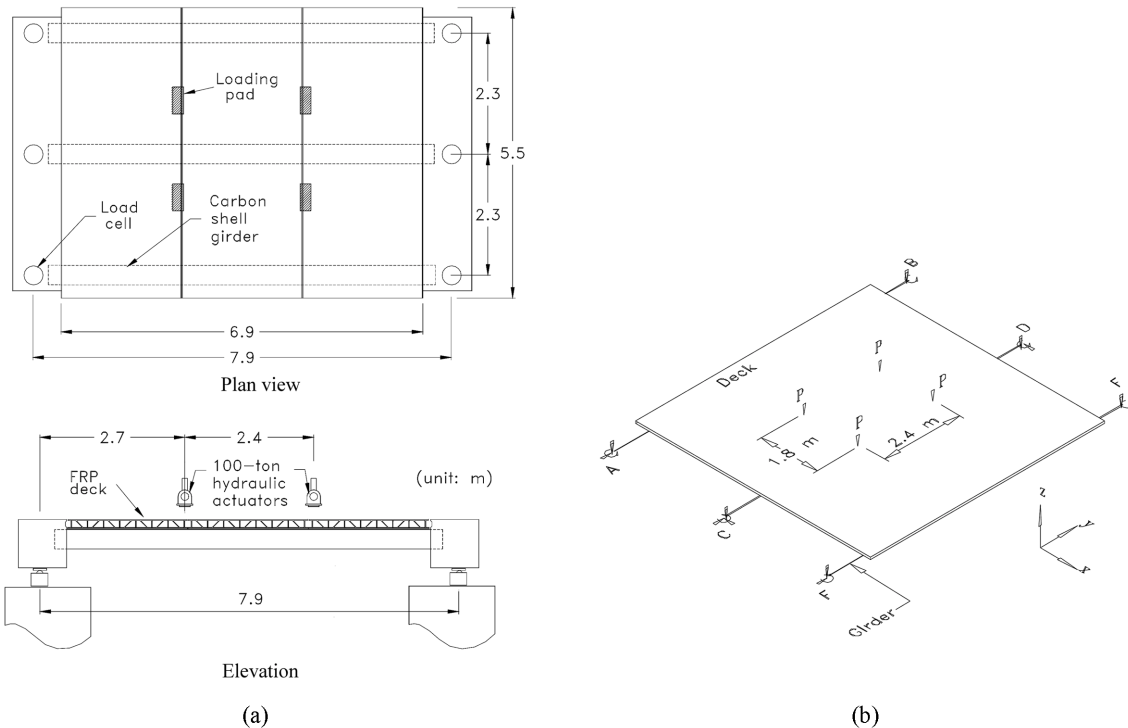


Fig. 7 (a) Schematic of the 3-girder sub assemblage test setup, (b) Schematic of layout and model boundary conditions

three translational DOFs. The non-linear constitutive relationship of the spring element is adopted from “push-out” tests, following earlier use in testing steel-concrete composite connections (Ollgaard *et al.* 1971). The specimen for the push-out test used in this investigation is described in detail in Zhao (1999) and Karbhari *et al.* (2000). The non-linear slippage relation which has a yield point is used as the constitutive relationship of the spring element.

The discretization of the deck panels and the girders is shown in Fig. 8(a) with a schematic of representative nodal arrangement being shown in Fig. 8(b). It is noted that in the actual system, shear connections between the deck and the girders are made with “U-shaped” dowels at every 0.6 m spacing, longitudinally. The spring elements in the FE model are therefore placed at every other cell of the deck. Between each set of adjacent spring elements a rigid link element is placed which maintains vertical displacement compatibility in the model (i.e., prevents the deck shell elements from “crashing into” the girder under vertical loads). The shell elements are modeled separately for flange and web sections with appropriate material properties for each. The reinforced concrete end blocks are modeled as beam elements with flexural and torsional rigidity with nodes of the elements being linked to the appropriate end supports by “rigid beam” elements. Since the experiment has a mixed boundary condition two different cases for connection of the deck panels to the support are considered so as to provide overall bounds of response. Case 1, simulating a rigid end provides the upper bound, assumes that the ends of both the deck and girders are rigidly connected to the end blocks thereby preventing any movement between the deck panels and end blocks. Case 2 assumes that the ends of the girders are rigidly connected to the end blocks but the

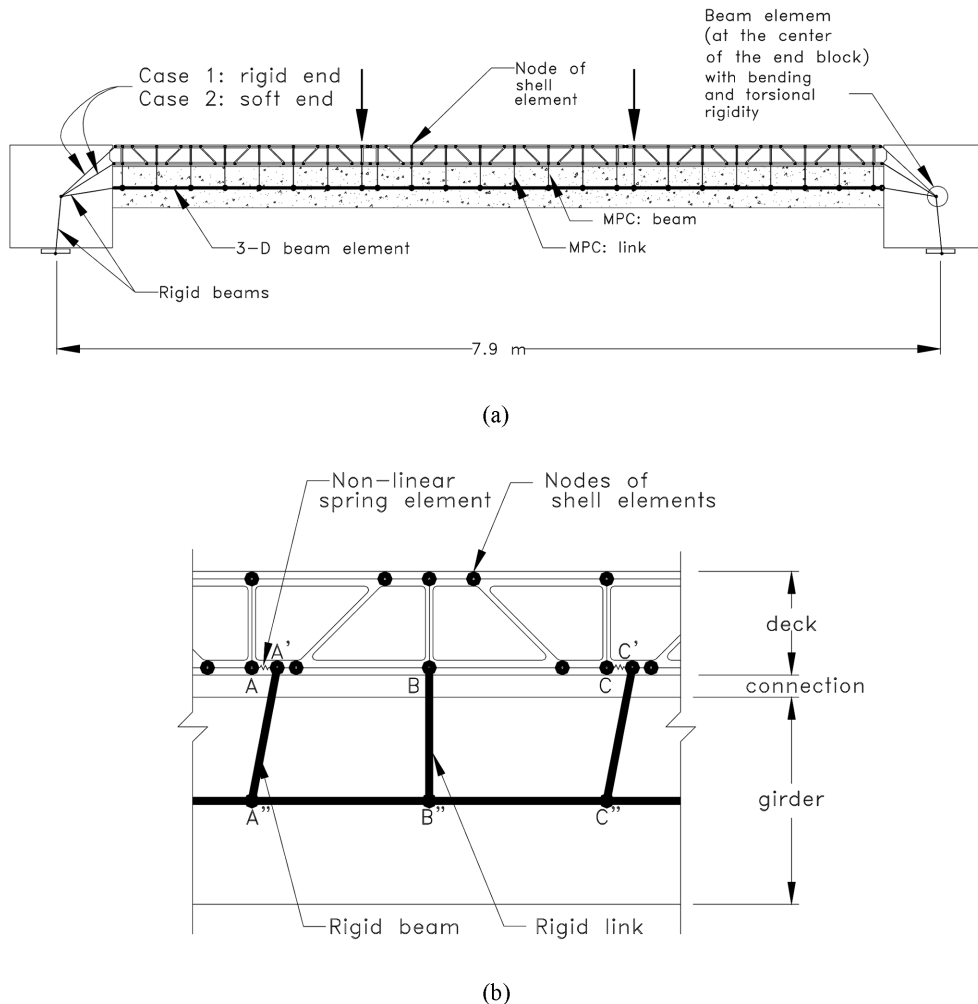


Fig. 8 (a) Overall system model, (b) Representative arrangement of nodes representing the girder and deck components

end of the deck is allowed relative movement against the girders, which increases the shear demand on the girder-to-deck connection, and provides the lower bound.

The total load versus center girder midspan deflection response envelopes of the sub-assembly obtained through application of the FE model are shown in Fig. 9. The stiffer curve corresponds to the rigid connection whereas the softer curve corresponds to the lower bound. Comparison of the value of in-plane stresses in the flange and web regions with the reduced smeared strengths defined earlier indicates that initiation of failure would be from the top flange of the deck panels in the girder direction at a load of 1990 kN. At this level the maximum compressive stress in the longitudinal direction of the top flange of the deck reaches the level of the reduced smeared strength ( $\sigma_s' = -65$  MPa, Table 3) in that direction. Stress levels at this load in other directions are significantly lower than the corresponding reduced smeared strength level. As shown in Fig. 5 failure is estimated to occur in ply 18 of the top flange under a compressive force causing

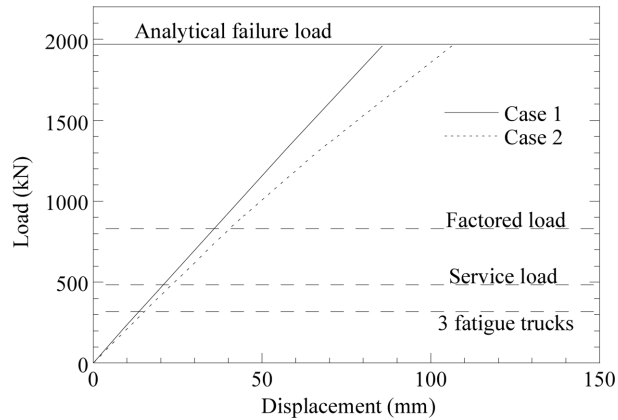


Fig. 9 Load-deflection bounds from the FEA models

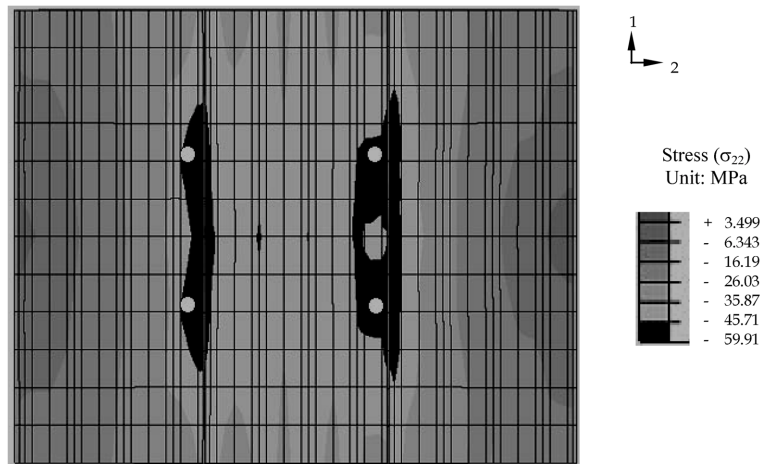


Fig. 10 FE generated in-plane stress contour of the top flange of the deck (in the girder direction of the system)

delamination. Globally, the locations of the maximum compressive stresses (shown as darker regions in Fig. 10) are distributed around the load introduction locations (shown as the four white circles) primarily due to longitudinal bending of the superstructure. It is also observed that there is inconsequential difference in the maximum compressive stress and failure mechanism at mid-span due to changes in end conditions (Cases 1 and 2, described earlier). While first-ply failure does not necessarily result in global failure, the mechanism of compressive failure initiated from an internal ply is likely to cause delamination within the flange and consequently cause a significant decrease in system stiffness.

#### 4. Experimental validation

The full-scale superstructure (described in detail in Karbhari *et al.* 2000) consists of three

longitudinal girders with an integral E-glass/vinylester-polyester deck system as shown in Fig. 11. Four servo-controlled hydraulic actuators were used to simultaneously apply flexural loads to the system, simulating the flexural and shear demands of the actual bridge. Application of two million cycles with a load of 56 kN at each actuator, to duplicate shear force demand on the prototype bridge at the girder-deck interface under full service loads, showed no signs of response degradation after initial settlement with very little change in system stiffness. Further stiffness characterization

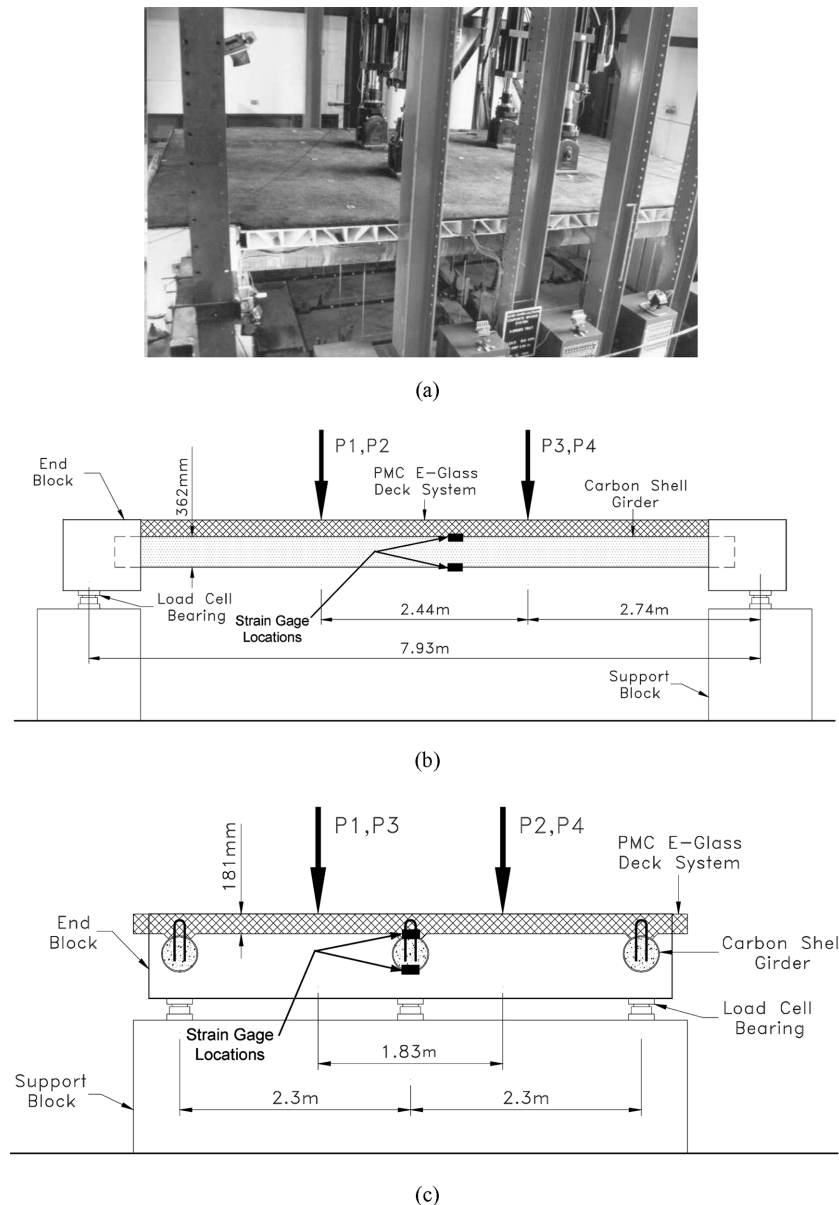


Fig. 11 3 girder-deck assemblage (Karbhari *et al.* 2000), (a) View of test, (b) Side-view of test setup geometry, (c) Cross-section of the test setup geometry

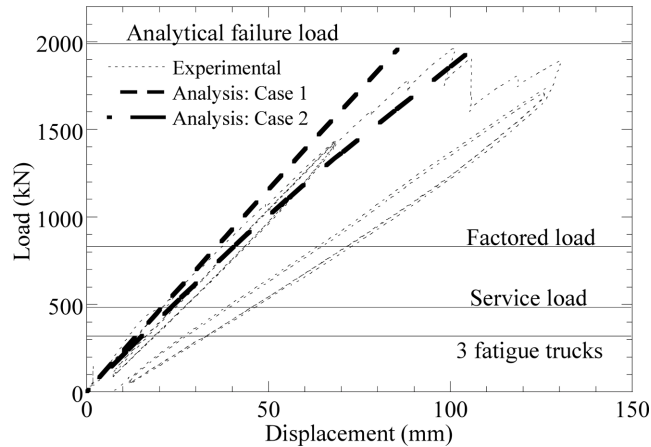


Fig. 12 Comparison of FE based response prediction and experimental load-deflection response (all at mid span under the central girder)

under combinations of load placement to consider other load combinations also showed no change in system stiffness (Karbhari *et al.* 2000).

For the purposes of failure characterization the assembly was loaded monotonically to failure keeping the load at all four actuators the same. As shown in Fig. 12, the load versus mid-span displacement relation was largely linear up to failure. Before failure, a slight load drop of approximately 40 kN was observed when the load reached 1750 kN. Although the load drop was accompanied by a breaking noise suggestive of fiber breakage or delamination in the composite, no visible damage to the deck was observed externally. The load-displacement relation maintained linear-elastic while more breaking noises were heard until global failure occurred at a total load of 1958 kN. At the global failure, it was observed that the top portion of the face sheet delaminated from the rest of the deck panel and buckled (Fig. 13). This type of failure is indicative of

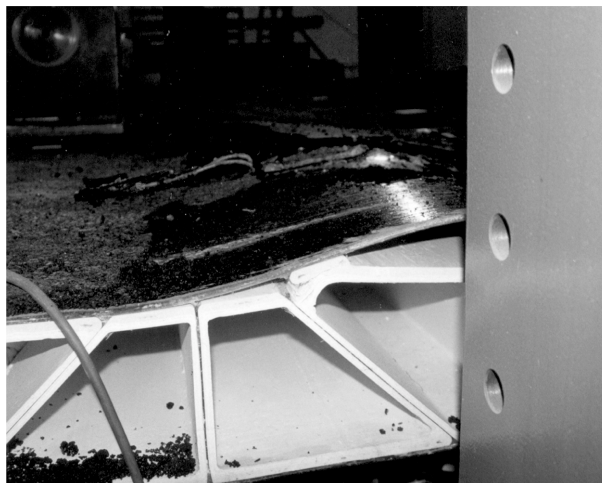


Fig. 13 Close-up of delamination failure in top flange

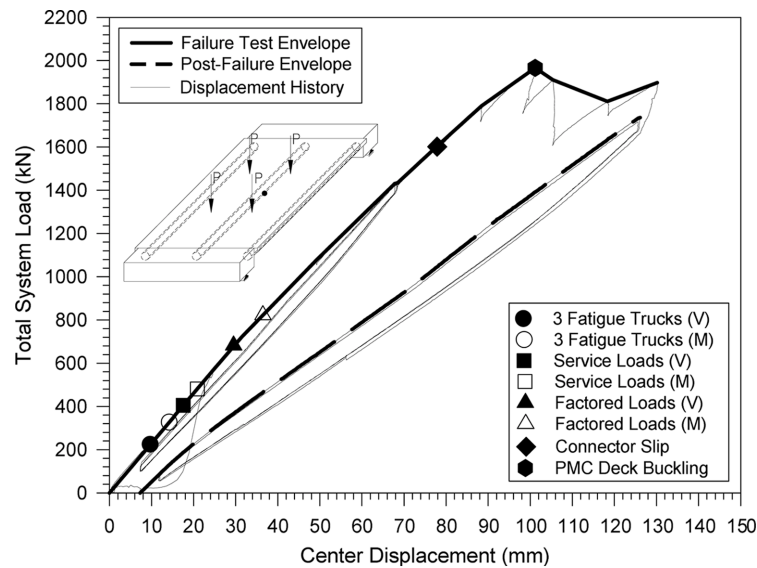


Fig. 14 Load-displacement event history based on middle girder response

delamination initiated by the failure of internal ply (or plies). While the failure was sudden and sounded dramatic (loud noise), the load drop immediately after the failure was merely 200 kN or 10% of the peak load. When loading continued, the system maintained virtually the same strength while an additional 60 mm of mid-span displacement was achieved. Loading was stopped at that point due to capacity limitations and safety concerns of the test setup. Post-test inspection of the specimen indicated that the delamination only occurred along the region of the highest compression stress (as shown in Fig. 10) that traversed the entire width of the specimen.

The experimental response measured at mid span falls between the upper and lower bounds of the FE model (Fig. 12), with failure taking place at a load of 1958 kN which is in excellent correlation with the analytical predicted value of 1990 kN. It is noted that the FE prediction of failure was associated with compressive failure in the top flange of the deck around the slotted cutouts causing delamination between reinforcement layers.

Fig. 14 shows the load-displacement response with indication of the key events during monotonic loading of the test unit. The figure also identifies the correspondence between the applied loads to the test units and the shear and moment demands on the prototype bridge system. After the deck failure the load was removed from the test unit and the system was loaded to a total load of 1780 kN for three cycles (unloading and loading). The system's response was linear elastic with a reduced stiffness, as indicated by the middle girder center displacement response envelopes shown in Fig. 14. Due to the local nature of the failure mode, the concrete filled girders remained intact. Thus, the system response was reduced to basically that of the girders alone. A comparison of the system secant stiffness values before and after failure using the middle girder center displacement as a representative parameter of the system shows that the reloading stiffness after failure is approximately 75% that of the initial stiffness.

## 5. Conclusions

A simplified method of analysis is proposed to incorporate effects of composite lamination and localized effects of geometric discontinuities such as cutouts in a FE analysis amenable to use by bridge designers. Stress demands obtained from the global FE models are compared with laminate-based predetermined reduced smeared strength levels to identify failure modes and locations based on the specific of composite geometry and configuration. The method is illustrated through a full-scale test of a 3 girder-deck assemblage and it is shown that load-deflection response, failure load, and mechanism can be accurately predicted through use of the method. The proposed methodology provides ease of use for conventional bridge designers while enabling the incorporation of aspects specific to FRP composites such as interlaminar stresses (which cause delaminations) and stress concentrations around cutouts.

## Acknowledgements

The authors would like to thank Ms. Lijuan “Dawn” Cheng for her assistance.

## References

- ASME-RTP-1d-1998 (1998), Addenda to ASME-RTP-1-1995 edition, Reinforced Thermoset Plastic Corrosion Resistant Equipment, *ASME*, New York, NY.
- Bakis, C.E., Bank, L.C., Brown, V.L., Cosenza, E., Davalos, J.F., Lesko, J.J., Machida, A., Rizkalla, S.H. and Triantafillou, T.C. (2002), “Fiber-reinforced polymer composites for construction – State-of-the-art review”, *J. Composites for Construction*, ASCE, **6**(2), 73-87.
- BS 4994 (1987), “British standard specification for design and construction of vessels and tanks in reinforced plastics”, *British Standards Institute*.
- Head, P.R. (1998), “Advanced composites in civil engineering – A critical review at this high interest, low use stage of development”, *Proc. of the 2nd Int. Conf. on Composites in Infrastructure*, **1**, Tucson, AZ, pp. 3015.
- Henry, J.A. (1985), “Deck girder systems for highway bridges using fiber reinforced plastics”, MS Thesis, North Carolina State University, Department of Civil Engineering.
- Hollaway, L.C. and Head, P.R. (2001), *Advanced Polymer Composites and Polymers in the Civil Infrastructure*, Elsevier, Oxford, UK.
- Karbhari, V.M. and Seible, F. (2000), “Fiber reinforced composites – Advanced materials for the renewal of civil infrastructure”, *Applied Composite Materials*, **7**(2/3), 95-124.
- Karbhari, V.M., Seible, F., Burgueno, R., Darol, A., Wernli, M. and Zhao, L. (2000), “Structural characterization of fiber-reinforced composite short - and medium - span bridge systems”, *Applied Composite Materials*, **7**, 151-182.
- Karbhari, V.M., Seible, F., Hegemier, G.A. and Zhao, L. (1997), “Fiber reinforced composite decks for infrastructure renewal – Results and issues”, *Proc. of the 1997 Int. Composites Exposition*, Nashville, TN, January, 3C/1-3C/6.
- Lekhnitskii, S.G. (1968), *Anisotropic Plates*, Gordon and Breach Science Publishers, New York.
- Lopez-Anido, R., GangaRao, H.V.S., Troutman, D. and William, D. (1998), “Design and construction of short-span bridges with modular FRP composite decks”, *Proc. of the 2nd Int. Conf. on Composites in Infrastructure*, Tucson, AZ, 634-644.
- Loud, S. and Kliger, H. (2001), Infrastructure Composites Report 2001, *Composites Worldwide*, Solana Beach, CA.
- Ollgaard, J.G., Slutter, R.G. and Fisher, J.W. (1971), “Shear strength of stud connectors in lightweight and

- normal-weight concrete”, *Eng. J.*, AISC, **8**(2), 55-64.
- Plecnik, J.M. and Azar, W.A. (1991), “Structural components, highway bridge deck applications”, *Int. Encyclopedia of Composites*, Eds. I. Lee and M. Stuart, **6**, 430-445.
- Seible, F., Karbhari, V.M. and Burgueno, R. (1999), “Kings stormwater channel and I-5/Gilman bridges, USA”, *Struct. Eng. Int.*, **9**(4), 250-253.
- Stone, D., Watkins, S., Nystrom, H. and Nanni, A. (2001), “Investigation of FRP materials for bridge construction”, *Proc. of the 5th National Workshop on Bridge Research in Progress*, Eds: C.K. Shield and A. E. Schultz, University of Minnesota, October, 145-150.
- Temeles, A.B. (2001), “Field and laboratory tests of a proposed bridge deck panel fabricated from pultruded fiber-reinforced polymer composites”, M.S. Thesis, submitted to the Department of Civil Engineering, Virginia Polytechnic Institute and State University.
- Vinson, J. and Sierakowski, R. (2002), *The Behavior of Structures Composed of Composite Materials*, Kluwer Academic Publishers, Dodrecht, Netherlands.
- Walker, H.S. (1998), “Fiberglass bridges and bridge decks”, *Proc. of the 2nd Int. Conf. on Composites in Infrastructure*, Tucson, AZ, 651.
- Zhao, L. (1999), “Characterization of deck-to-girder connections in FRP composite superstructures”, Ph.D. dissertation, submitted to the Department of Structural Engineering, University of California, San Diego.
- Zureick, A.H., Shih, B. and Munley, E. (1995), “Fiber-reinforced polymeric bridge decks”, *Struct. Eng. Review*, **7**(3), 257-266.